Comparison of μCT, MRI and Optical Reflectance Imaging for Assessing the Growth of GFP/RFP-expressing Tumors

LOTFI ABOU-ELKACEM[1], FELIX GREMSE[1], STEFAN BARTH[2,3], ROBERT M. HOFFMAN[4,5], FABIAN KIESSLING[1] and WILTRUD LEDERLE[1]

[1]*Department of Experimental Molecular Imaging, Medical Faculty, RWTH Aachen University, Aachen, Germany;*
[2]*Department of Experimental Medicine and Immunotherapy, Institute for Applied Medical Engineering, Aachen, Germany;*
[3]*Department of Pharmaceutical Product Development, Fraunhofer Institute for Molecular Biology and Applied Ecology, Aachen, Germany;*
[4]*Department of Surgery, University of California, San Francisco, CA, U.S.A.;*
[5]*AntiCancer Inc., San Diego, CA, U.S.A.*

Abstract. *Aim: To compare magnetic resonance imaging (MRI), micro-computed tomography (μCT), optical reflectance imaging (ORI) and caliper measurements for subcutaneous tumor detection and size assessment. Materials and Methods: HCT 116-green- (GFP)-red-fluorescent protein (RFP) tumor volumes were measured in vivo by calipers and by ORI, MRI and μCT over 15 days and validated ex vivo. The method correlating best with the ex vivo tumor volumes was used as reference for longitudinal in vivo correlations. Results: MRI and ORI detected tumors at day 1 post-injection, μCT after 3 days. The in vivo MRI data correlated best with the ex vivo tumor volumes (r^2=0.96), followed by μCT (r^2=0.93). Thus, MRI was chosen as the reference. μCT- (r^2=0.90), in vivo caliper data (r^2=0.80) and fluorescence intensities (GFP:r^2=0.71; RFP:r^2=0.75) highly correlated with MRI-data, whereas fluorescent areas (GFP:r^2=0.26; RFP:r^2=0.30) poorly correlated. Conclusion: MRI sensitively detects tumors and precisely determines their size; μCT is an accurate alternative for larger tumors; ORI is as sensitive as MRI, but overestimates small tumor sizes; and fluorescence intensity correlates better with tumor volume than fluorescence area.*

In cancer research, calipers measurements are still often used for assessing tumor size in mouse models (1). However, caliper measurements only allow the assessment of two dimensions, are only applicable for subcutaneous (*s.c.*) tumors and are highly dependent on the experimenter (2). Furthermore, viable and non-viable tumor tissue cannot be differentiated. Non-invasive imaging by magnetic resonance (MR), computed tomography (CT) and optical reflectance imaging (ORI) also plays an important role for tumor detection, staging and therapy monitoring. All these imaging modalities allow longitudinal analyses on the same animal, providing individual information about the disease or therapy course. Additionally, the number of animals and study costs can be reduced (3-6). However, parameters such as sensitivity, specificity, accuracy and three-dimensional morphology, as well as costs and examination time have to be considered when choosing the appropriate modality.

The imaging modalities, which are applied for assessing tumor growth, depend on the tumor model, the duration of the measurement and the availability of imaging systems. However, the imaging modalities differ in their strengths and limitations. Magnetic resonance imaging (MRI) and micro-computed tomography (μCT) have deep penetration. MRI also provides good soft-tissue contrast and high spatial resolution, but is time consuming and expensive. μCT is usually faster and less expensive than MRI, offers good spatial resolution, but has less soft tissue contrast. In addition, increased resolution with μCT requires higher radiation doses. Despite limited penetration depth, ORI has a very high sensitivity for detecting fluorescent probes, such as fluorescent proteins (6-8).

In pre-clinical studies, fluorescence imaging is often used for tumor staging and therapy monitoring. For instance, fluorescence imaging of cancer xenografts expressing green- (GFP) or red-fluorescent protein (RFP) allows the visualization of tumor growth, progression, metastases and therapy efficacy (6, 7).

Correspondence to: Dr. Wiltrud Lederle, Department of Experimental Molecular Imaging, Medical Faculty, RWTH Aachen University, D-52074 Aachen, Germany. Tel: +49 2418080116, Fax: +49 241803380116, e-mail: wlederle@ukaachen.de

Key Words: Magnetic resonance imaging, micro-computed tomography, optical reflectance imaging, tumor volume, molecular imaging, GFP, RFP.

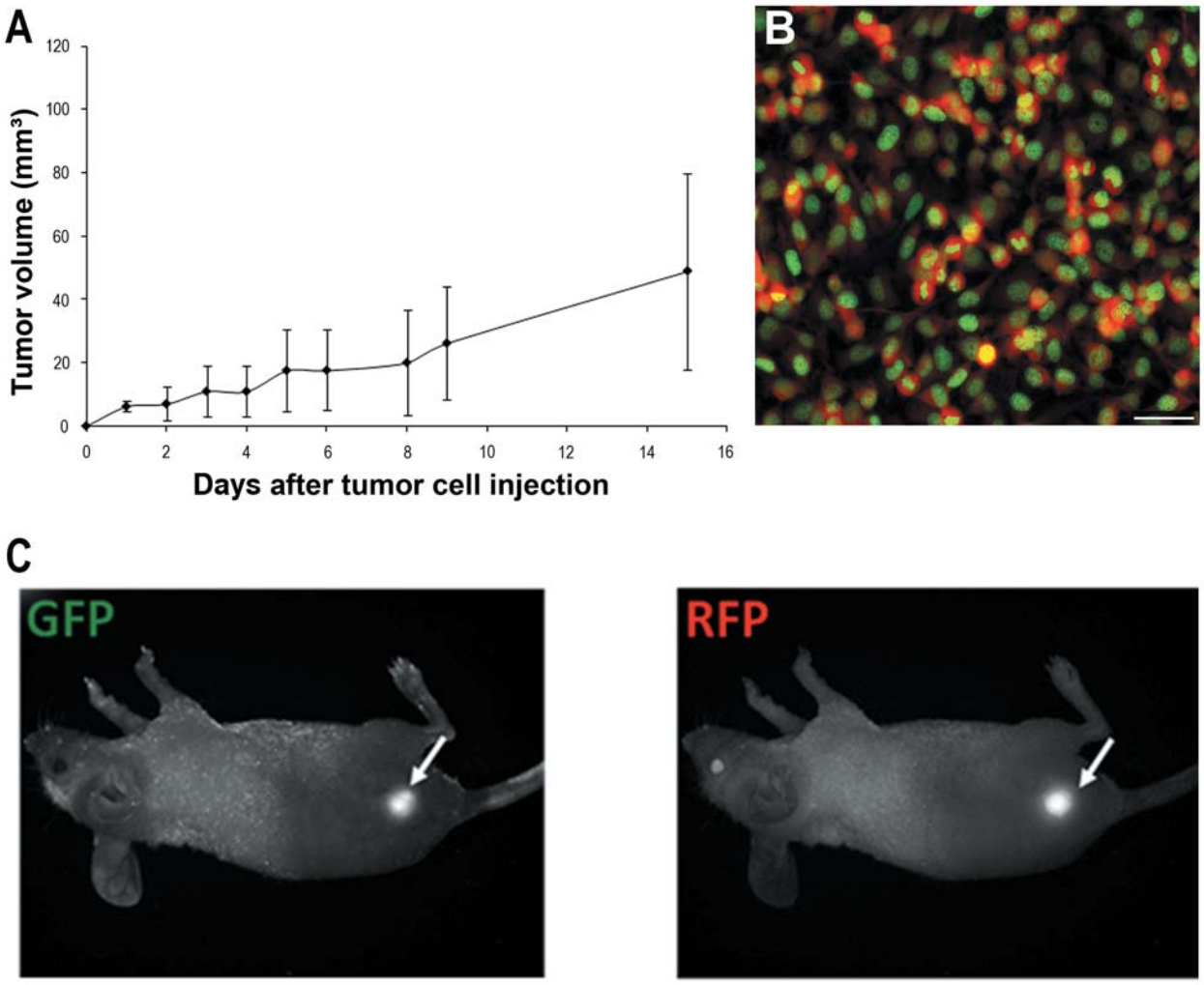

Figure 1. *A: Tumor growth curve of subcutaneously-growing HCT 116-GFP-RFP xenografts in nude mice. Mean tumor volumes (±SD) of six animals at definite time-points after tumor cell injection determined by caliper in vivo. B: Dual-color fluorescence image of green- (GFP) and red fluorescent protein (RFP)-expressing colon cancer cells (HCT 116-GFP-RFP) in vitro. Scale bar=100 μm. C: Unmixed fluorescence images of a representative mouse one day after cell injection. Arrows mark the s.c. HCT 116-GFP-RFP tumors.*

In the present report, the accuracy and sensitivity of MRI, μCT, ORI and caliper measurements were compared for early tumor detection and tumor growth assessment, using double-transfected human colon cancer HCT 116-GFP-RFP subcutaneously-growing xenografts in nude mice.

Materials and Methods

The tumor model. The double transfected human colon cancer cell line HCT 116-GFP-RFP stably expresses GFP in the nucleus and RFP in the cytoplasm and was supplied by AntiCancer Inc. (San Diego, CA, USA). The cells were cultivated in RPMI 1560 medium (Gibco®, Invitrogen GmbH, Darmstadt, Germany) containing 10% fetal bovine serum (Gibco®), 1% penicillin/ streptomycin (Gibco®) and 400 μg/mL Genetecin (Gibco®).

Animal experiments. All the experiments were approved by the Governmental Review Committee on Animal Care. Human colon carcinoma xenografts were implanted by *s.c.* injection of 2×10^6 HCT 116-GFP-RFP cells in 100 μL PBS into the right flank of 6-8 week old female CD1-nude mice (Charles River, Sulzfeld, Germany). A total of nine mice were included in the study. In six mice, tumor size was determined daily by caliper measurements in two dimensions. In addition, the tumor size of these six mice was assessed every second day using the non-invasive imaging modalities MRI, ORI and μCT starting from day 1 after tumor inoculation. The measurements were continued for 15 days after tumor inoculation. At day 15 post-injection, all six longitudinally measured mice were sacrificed. The tumors were resected and the skin over the tumors was removed. The tumors were excised and their volumes determined *ex vivo* in order to determine the non-invasive imaging modality that correlated best with *ex vivo* tumor size. For better validation, three additional

animals were sacrificed at day 12 post-injection in order to include smaller tumor sizes for comparison.

For non-invasive imaging, the animals were anesthetized by inhalation of a mixture of isoflurane (1.5 %) and O_2.

Optical reflectance imaging. *In vivo* fluorescence imaging was performed with a CRi Maestro imaging system (CRi Inc., Woburn, MA, USA), using a blue filter set in the multi-filter acquisition mode (500-720 nm; 10 nm increment) and an exposure time of 500 msec. A cooled charge-coupled device (CCD) camera (Sony ICX285, Yokohama, Japan) was used for sensitive photon detection. The threshold setup for all the image analyses was fixed immediately after tumor injection of fluorescent HCT 116-GFP-RFP cells and kept constant for the whole experiment. Before each animal experiment, GFP- and RFP-spectra were recorded which served as pre-information for spectral unmixing and thus allowed a better separation of GFP and RFP signals from the background. Fluorescence tumor area (FA) and total fluorescence intensity (FI) were determined by the CRi software using the unmixed GFP and RFP images.

Magnetic resonance imaging (MRI). MRI data were acquired on a clinical 3 Tesla whole body scanner (Achieva 3.0 T, Philips, Brest, Netherlands). A small animal solenoid receiver coil (Philips, Hamburg, Germany) with an integrated heating system to regulate the temperature of the mice was used for signal acquisition. The MR protocol started with a short survey scan for choosing the field of view (FOV) followed by transversal T1- and T2-weighted sequences. The imaging parameters in the transversal direction were: T1-weighted (T1w) spin echo sequence: repetition time (TR) 700 msec, echo time (TE) 13 msec, FOV 30 mm × 30 mm × 43.9 mm, matrix 148×150, slice thickness 1 mm, slice gap 0.1 mm, voxel size 0.2 mm × 0.2 mm × 1.0 mm; T2-weighted (T2w) turbo spin echo sequence: TR 4781 msec, TE 100 msec, turbo spin echo factor (TSE factor) 10, flip angle 90˚, number of signal averages (NSA) 3, FOV 30 mm × 30 mm × 43.9 mm, matrix 148×150, slice thickness 1 mm, voxel size 0.2 × 0.2 × 1.0 mm. The same sequences were followed in the sagittal direction: T1w spin echo sequence: TR 700 msec, TE 13 msec, FOV 90 mm × 25.7 mm × 28.5 mm, matrix 448 × 126, slice thickness 1 mm, slice gap 0.1 mm, voxel size 0.2 mm × 0.2 mm × 1.0 mm; T2w turbo spin echo sequence: TR 4781 msec, TE 100 msec, FOV 90 mm × 25.7 mm × 28.5 mm, matrix 448×126, slice thickness 1 mm, voxel size 0.2 mm × 0.2 mm × 1.0 mm. The total scan time was approximately 30 minutes.

Micro computed tomography (μCT). μCT scans were performed using the dual source μCT system Tomoscope Duo (CT Imaging GmbH, Erlangen, Germany). The following scan protocol was used: both tubes ran at energies of 40 kV, 1 mA and the exposure dose was 344 mGy per scan. Each flat panel detector acquired 720 projections at 5 frames per second (fps). The scan time was 90 sec per mouse in the transversal orientation. Images were reconstructed with a Feldkamp algorithm using a soft reconstruction kernel (T10) and isotropic voxel sizes of 70 μm. The field of view was 42 mm × 35 mm × 30.8 mm.

Determination of the tumor volumes. Whereas ORI and caliper measurements allow determination of the FA or the tumor diameter in two dimensions, MRI and μCT allow the acquisition of 3-dimensional data including tumor depth. Tumor volumes were calculated assuming the tumors to have an ellipsoid shape: Caliper, ORI: $a \times b^2 \times \pi/6$; MRI, μCT: $a \times b \times c \times \pi/6$, where a represents tumor length, b, tumor width and c, tumor depth.

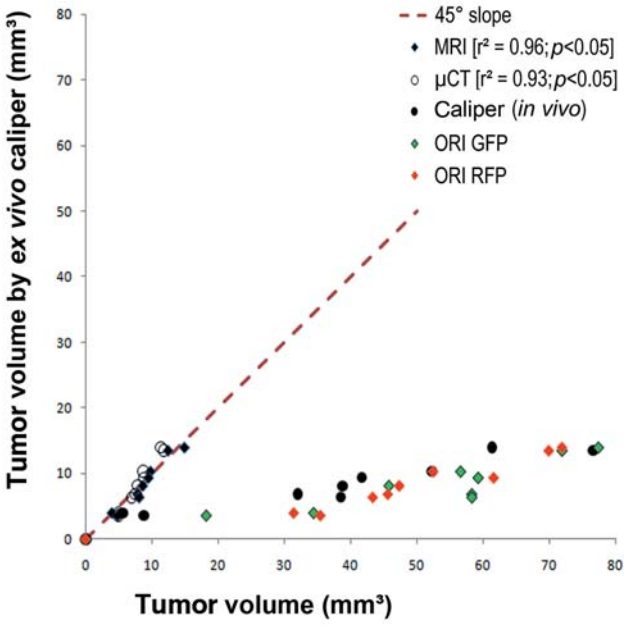

Figure 2. *Correlation of the tumor volumes determined in vivo by MRI, μCT, caliper and optical reflectance imaging (ORI) (GFP, RFP) with ex vivo caliper data at day 12 and 15; n=9.*

Data analysis and statistics. The modality which provided the most congruent tumor volume data with the *ex vivo* data was first determined. Then, the tumor volumes obtained by the other modalities were compared with the results from this best-performing modality. Pearson's correlation coefficients (r) and significance of correlation were determined (as indicated within the corresponding graphs). The significances for differences between correlations were tested using the Fisher *z*-test and $p<0.05$ was considered statistically significant.

Results

Tumor growth. The tumor size assessment of the *s.c.* xenografts by caliper measurements demonstrated a constant increase in tumor volumes (Figure 1A). The HCT 116-GFP-RFP cells give a bright green fluorescence signal in the nucleus and an intense red signal in the cytoplasm, as shown by fluorescence microscopy (Figure 1B), allowing *in vivo* detection by ORI at day 1 post-injection (Figure 1C).

Correlation of ex vivo tumor size measurements with in vivo data. In order to correlate the various modalities for tumor size assessment, all the tumor volumes determined by MRI, μCT and ORI *in vivo* at days 12 and 15 post-injection were compared with the corresponding *ex vivo* data. The *ex vivo* tumor volumes significantly correlated with the *in vivo* MRI- (r^2=0.96, $p<0.05$) and μCT-data (r^2=0.93, $p<0.05$) (Figure 2). In addition, the MRI- and *ex vivo* data pairs almost lay on the 45˚ linear slope in the graph with equally scaled x-

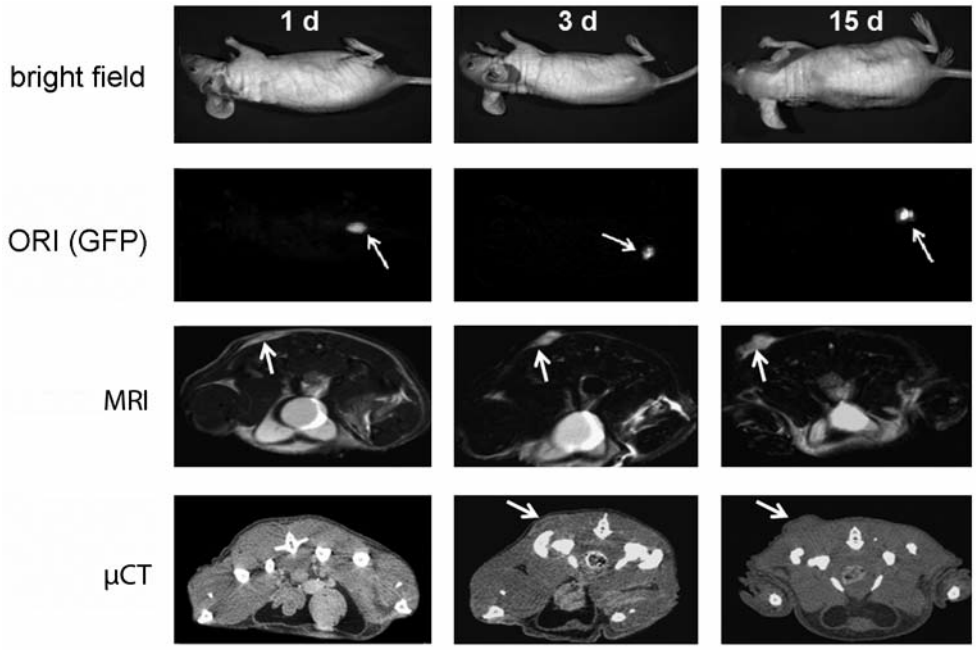

Figure 3. *Monitoring of tumor growth in s.c. HCT 116-GFP-RFP xenografts using optical reflectance imaging (ORI), MRI and µCT. Representative images show xenograft tumors 1, 3 and 15 days after cell injection. Arrows mark the s.c. HCT 116-GFP-RFP tumors.*

and y-axes. This demonstrated the high congruency of the values. µCT- and *ex vivo* data were slightly less congruent. In contrast, *in vivo* caliper measurements and ORI resulted in higher tumor volumes, as seen by the right shift of the correlation values (Figure 2). Consequently, the non-invasively measured tumor volumes were correlated with the results obtained by MRI.

Sensitivity for tumor detection and accuracy in the assessment of tumor growth. All the modalities showed a high sensitivity for initial tumor detection (Figure 3). However, only ORI and MRI detected the HCT 116-GFP-RFP tumors by one day after tumor cell injection. However, non-contrast-enhanced µCT did not allow tumor detection until day 3 post-injection. No difference in the sensitivity for initial tumor detection was observed between GFP and RFP imaging. When the µCT, caliper, and ORI data were correlated with MRI, the highest correlation was found between the MRI- and µCT data (Figure 4A; r^2=0.90; p<0.05). *In vivo* caliper data showed a high correlation with the MRI data (Figure 4B; r^2=0.80; p<0.05). Additionally, a high correlation was found between FI data and the MRI-measurements (Figure 4C-D; RFP: r^2=0.75; p<0.05; GFP: r^2=0.71; p<0.05). The FA and fluorescence volume measurements showed a low correlation with the MRI data (Figure 4E-H; FA RFP: r^2=0.30; p<0.05; GFP: r^2=0.26; p<0.05 and fluorescence volume; RFP: r^2=0.40; p<0.05; GFP: r^2=0.34; p<0.05). The tumor area and volume were greater when measured by ORI at the early time-points after tumor inoculation. This result was comparable for both fluorescent proteins (GFP and RFP). Statistical analyses of the correlation graphs using the Fisher *z*-test revealed significant differences between the MRI/CT *versus* MRI/FI and the MRI/CT *versus* MRI/FA as well as the MRI/CT and MRI/fluorescence volume graphs (MRI/CT *vs*. MRI/FI [RFP]: p=0.045; MRI/CT *vs*. MRI/FI [GFP]: p=0.02; MRI/CT *vs*. MRI/FA [RFP]: p<0.001; MRI/CT *vs*. MRI/FA [GFP]: p<0.001; MRI/CT *vs*. MRI/volume [RFP]: p<0.001; MRI/CT *vs*. MRI/volume [GFP]: p<0.001.

Discussion

For all the determined time-points after tumor inoculation, the tumor volumes measured by µCT correlated best with the corresponding MRI data, which in turn had the highest correlation and congruency for the tumor volume, when compared to *ex vivo* measurements with calipers. In comparison to µCT, the ability of MRI for detecting and determining the size of small tumors was most probably related to the better tumor demarcation.

In MRI, the strong signal in T2-weighted sequences derives from intra- and extracellular edema and the high cellularity (9). In contrast, X-ray attenuation is not considerably different between tumor cells, edema and cells of the surrounding tissue

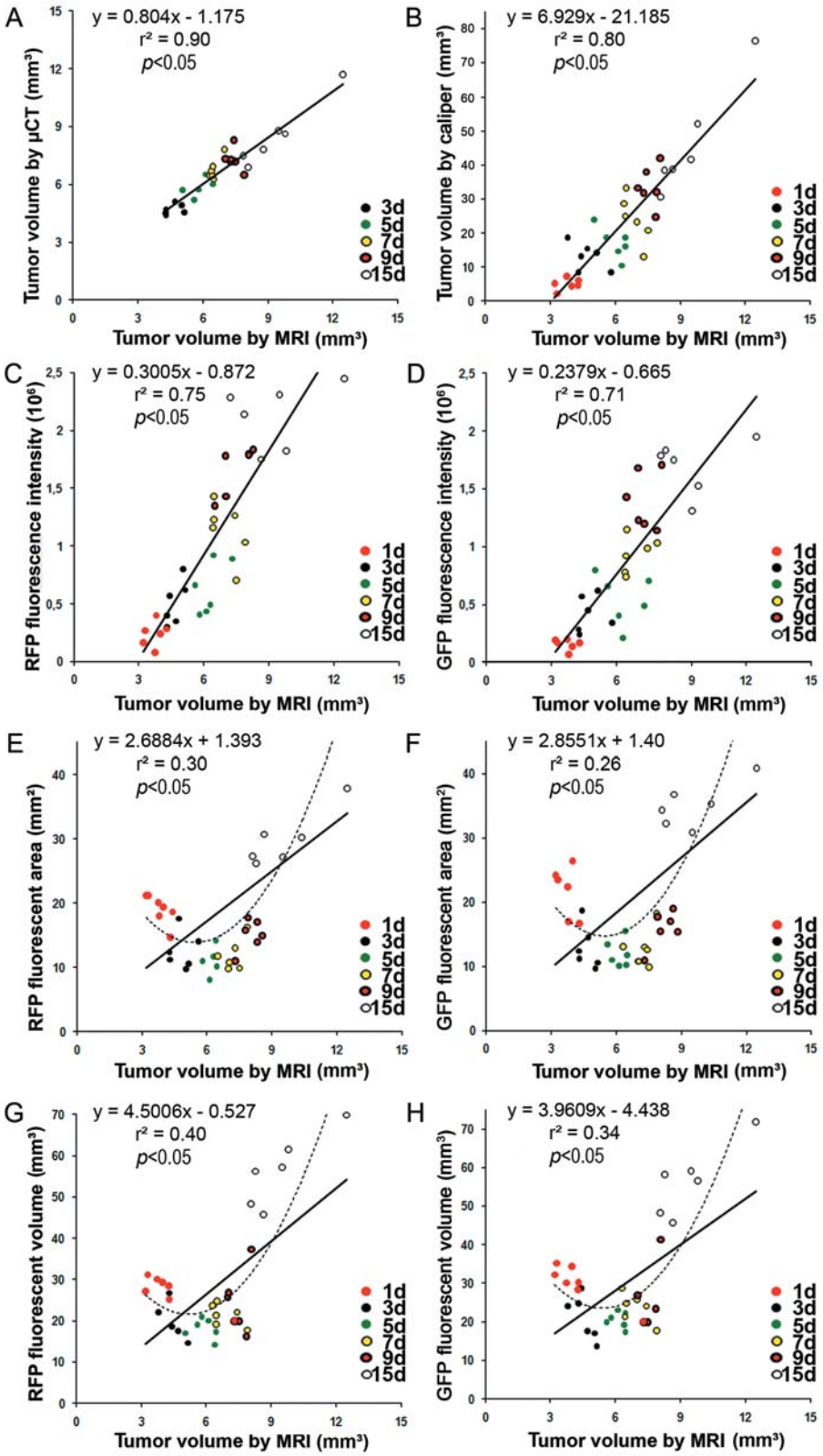

Figure 4. *Correlation of tumor volumes determined in vivo by MRI with tumor volumes measured by µCT (A), calipers (B) and optical reflectance imaging. (ORI) fluorescence intensities (C-D), fluorescent areas (E-F) and fluorescent volume (G-H) measured from 1-15 days (1d-15d) after tumor cell injection. Solid line: linear regression line, dashed line=square polynomial trend line.*

(10). Therefore, tumor detection by μCT becomes possible at later time-points (from day 3 post-injection compared to day 1 for MRI and ORI), when a capsule has formed and the tumor is surrounded by sufficient neo-stroma. Although non-contrast-enhanced μCT was less sensitive than MRI, the good correlation with the MRI data suggested that μCT could be used for rapid assessment of tumor growth when the tumor is large enough. Sensitivity in μCT can be increased using intravenous contrast agents. Nevertheless, due to the high viscosity of CT contrast agents and thus the high pressure needed for its injection, there is a significant risk of vascular rupture and paravasal deposition in small animals (11). Moreover, catheterization of a mouse takes about 5-10 min which slows longitudinal studies with high animal numbers. Frequent catheterization of the animals, also, leads to scar formation at the tail vein and increasingly difficult catheterization. It should also be noted that most pre-clinical contrast agents show significant toxicity. In addition, repeated μCT-measurements lead to an accumulation of radiation doses. The lethal dose for a mouse, depending on strain and age, ranges from 5 to 7.6 Gy (12). The risk of a lethal radiation dose can be minimized by using protocols that are optimized for sufficient spatial resolution with a minimal radiation dose as used in the present study (344 mGy).

In vivo caliper measurements and ORI resulted in larger tumor volumes, which was particularly relevant for small tumors assessed by ORI. The main limitations include the lack of a precise definition of the tumor borders (13-15). However, caliper measurements still measure changes in tumor size over time, and the data showed a high correlation with the MRI data throughout the whole observation period. For ORI, fluorescence intensity measurements in contrast to fluorescence area and volume also showed a good correlation with the MRI data. In ORI, accurate signal localization is affected by light scattering within the tissue. Injecting the same number of cells distributed like a disc compared with a spheroid leads to comparable intensities, but not to similar areas. In addition, a spheroid localized directly under the skin appears as a small intense round structure, but if localized only a few millimeters deeper, it appears as a less intense but larger spot at the surface due to scattering of photons. In contrast, the overall light intensity is less affected.

Although tissue absorption is dependent on the wavelength, no differences were observed between GFP and RFP measurements. This might be explained by the superficial localization of the tumors. Katz *et al*. (16) found a very high correlation between non-invasive ORI in live mice with orthotopic RFP-expressing pancreatic tumors and tumor volume measured by caliper *ex vivo*. A high correlation was also found between non-invasive *in vivo* ORI-measurements and MRI in the same orthotopic pancreatic model as well as an esophageal cancer model (17, 18). Far-red proteins, such as mCherry, Katushka and mPlum or near-infrared fluorescent proteins, for example eqFP670, may confer advantages for deeper imaging (19, 20). Near-infrared fluorescence (NIRF) imaging allows a higher penetration depth, since absorption and autofluorescence of the tissue are minimal in this wavelength range (5, 8). In this context, tomographic fluorescence should allow better localization and quantification of deeply localized lesions (21, 22). Future studies with these modalities should be very important for the understanding of *in vivo* tumor biology.

In conclusion, MRI is highly sensitive for tumor detection and correlates best with *ex vivo* tumor measurement with caliper; μCT is a rapid method of measuring tumors of larger sizes and optical imaging of RFP/GFP fluorescence intensity rather than fluorescence area, is highly sensitive for detecting GFP/RFP-expressing tumor cells, but the correlation with *ex vivo* caliper measurement of tumor volume is less than MRI for the *s.c*. tumors studied in the present report.

Acknowledgements

This work was supported by the Deutsche Forschungsgemeinschaft (KI 1072/2-1) and by High Tech NRW (ForSaTum).

References

1 Tomayko MM and Reynolds CP: Determination of subcutaneous tumor size in athymic (nude) mice. Cancer Chemother Pharmacol *24*: 148-154, 1989.

2 Euhus DM, Hudd C, LaRegina MC and Johnson FE: Tumor measurement in the nude mouse. J Surg Oncol *31*: 229-234, 1986.

3 McDonald DM and Choyke PL: Imaging of angiogenesis: from microscope to clinic. Nat Med *9*: 713-725, 2003.

4 Cha S, Johnson G, Wadghiri YZ, Jin O, Babb J, Zagzag D and Turnbull DH: Dynamic, contrast-enhanced perfusion MRI in mouse gliomas: correlation with histopathology. Magn Reson in Med *49*: 848-855, 2003.

5 Weissleder R and Pittet MJ: Imaging in the era of molecular oncology. Nature *452*: 580-589, 2008.

6 Hoffman RM: The multiple uses of fluorescent proteins to visualize cancer *in vivo*. Nat Rev Cancer *5*: 796-806, 2005.

7 Hoffman RM: Green fluorescent protein imaging of tumour growth, metastasis, and angiogenesis in mouse models. Lancet Oncol *3*: 546-556, 2002.

8 Weissleder R and Ntziachristos V: Shedding light onto live molecular targets. Nat Med *9*: 123-128, 2003.

9 Santamaría G, Velasco M, Bargalló X, Caparrós X, Farrús B and Luis Fernández P: Radiologic and pathologic findings in breast tumors with high signal intensity on T2-weighted MR images. Radiographics *30*: 533-548, 2010.

10 Badea CT, Drangova M, Holdsworth DW and Johnson GA: *In vivo* small animal-imaging using micro-CT and digital subtraction angiography. Phys Med Biol *53*: R319-R350, 2008.

11 Dawson P, Cosgrove DO and Grainger RG: Textbook of Contrast Media (Dawson P, Cosgrove DO, Grainger RG (eds.). Oxford, Informa Healthcare, pp. 95-120, 1999.

12 Sato F, Sasaki S, Kawashima N and Chino F: Late effects of whole or partial body x-irradiation on mice: life shortening. Int J Radiat Biol Relat Stud Phys Chem Med *39*: 607-615, 1981.
13 Ishimori T, Tatsumi M and Wahl RL: Tumor response assessment is more robust with sequential CT scanning than external caliper measurements. Acad Radiol *12*: 776-781, 2005.
14 Massoptier L and Casciaro S: A new fully automatic and robust algorithm for fast segmentation of liver tissue and tumors from CT scans. Eur Radiol *18*: 1658-1665, 2008.
15 Ayers GD, McKinley ET, Zhao P, Fritz JM, Metry RE, Deal BC, Adlerz KM, Coffey RJ and Manning HC: Volume of preclinical xenograft tumors is more accurately assessed by Ultrasound imaging than manual caliper measurements. J ultrasound Med *29*: 891-901, 2010.
16 Katz MH, Takimoto S, Spivack D, Moossa AR, Hoffman RM and Bouvet M: A novel red fluorescent protein orthotopic pancreatic cancer model for the preclinical evaluation of chemotherapeutics. J Surg Res *113*: 151-160, 2003.
17 Bouvet M, Spernyak J, Katz MH, Mazurchuk RV, Takimoto S, Bernacki R, Rustum YM, Moossa AR and Hoffman RM: High correlation of whole-body red fluorescent protein imaging and magnetic resonance imaging on an orthotopic model of pancreatic cancer. Cancer Res *65*: 9829-9833, 2005.
18 Gros SJ, Dohrmann T, Peldschus K, Schurr PG, Kaifi JT, Kalinina T, Reichelt U, Mann O, Strate TG, Adam G, Hoffman RM and Izbicki JR: Complementary use of fluorescence and magnetic resonance imaging of metastatic esophageal cancer in a novel orthotopic mouse model. Int J Cancer *126*: 2671-2681, 2010.
19 Shcherbo D, Merzlyak EM, Chepurnykh TV, Fradkov AF, Ermakova GV, Solovieva EA, Lukyanov KA, Bogdanova EA, Zaraisky AG, Lukyanov S and Chudakov DM: Bright far-red fluorescent protein for whole-body imaging. Nat Methods *4*: 741-746, 2007.
20 Shcherbo D, Shemiakina II, Ryabova AV, Luker KE, Schmidt BT, Souslova EA, Gorodnicheva TV, Strukova L, Shidlovskiy KM, Britanova OV, Zaraisky AG, Lukyanov KA, Loschenov VB, Luker GD and Chudakov DM: Near-infrared fluorescent proteins. Nat Methods *7*: 827-829, 2010.
21 Ntziachristos V, Tung CH, Bremer C and Weissleder R: Fluorescence molecular tomography resolves protease activity *in vivo*. Nat Med *8*: 757-760, 2002.
22 Björn S, Ntziachristos V and Schulz R: Mesoscopic epifluorescence tomography: reconstruction of superficial and deep fluorescence in highly-scattering media. Opt Express *18*: 8422-8429, 2010.

Received May 23, 2011
Revised July 14, 2011
Accepted July 15, 2011